

# Functional Characterization and Comparison of the Outer Blood–Retina Barrier and the Blood–Brain Barrier

Heiko Steuer,<sup>1</sup> Andreas Jaworski,<sup>1</sup> Bernd Elger,<sup>2</sup> Martin Kaussmann,<sup>3</sup> Jörg Keldenich,<sup>3</sup> Herbert Schneider,<sup>2</sup> Dieter Stoll,<sup>1</sup> and Burkhard Schlosshauer<sup>1</sup>

**PURPOSE.** To determine efflux systems of the outer blood–retina barrier (oBRB) and compare the oBRB with the blood–brain barrier (BBB).

**METHODS.** Porcine oBRB structure and transport characteristics of freshly dissected intact tissue sheets were investigated with scanning electron microscopy, immunocytochemistry, vital dye labeling, and pharmacological agents, using HPLC/mass spectrometry. To compare drug permeation across the oBRB and the BBB, three different systems were used: (1) oBRB tissue sheets in a two-chamber device in vitro; (2) an in vitro BBB model composed of purified astrocytes and brain capillary endothelial cells on transfilter membranes; and (3) an in vivo model based on the brain–plasma ratio of drugs in mice.

**RESULTS.** Efflux pumps (multidrug resistance protein [P-gp] and multidrug resistance-associated protein [MRP]) were demonstrated by antibody staining. Side-specific application of three P-gp and MRP substrates and selective transport inhibition suggested that both membrane proteins were preferentially located on the choroidal side of the oBRB. Therefore, the efflux was directed toward the blood, as in the BBB. To relate the transport characteristics of the oBRB to the BBB, up to nine different test compounds were used. The ranking of the permeability coefficients ( $P_c$ ) and the brain–plasma ratios of test compounds indicated that the oBRB has barrier and carrier features similar to those of the BBB in vitro and in vivo.

**CONCLUSIONS.** Despite the fact that epithelial oBRB and endothelial BBB have developed as separate entities with many site-specific functions, their transport and permeation characteristics display surprising similarities, that include the polar-

ized expression of the two major efflux pumps P-gp and MRP. (*Invest Ophthalmol Vis Sci.* 2005;46:1047–1053) DOI:10.1167/iops.04-0925

Both retinal and brain neurons depend on a stringently controlled homeostasis. In both cases, blood barriers (albeit structurally different) prevent adverse effects that could arise from changes in the composition of the nurturing blood, such as excitotoxic concentrations of glutamate.<sup>1</sup> The retinas of some mammals including humans and pigs possess elaborate capillaries with barrier characteristics (inner blood–retina barrier, iBRB), whereas the neural retina of other species (e.g., horses and rabbits) is essentially devoid of retinal vasculature. The rabbit retina blood vessels, in particular, are evident only in the restricted area of the so-called visual streak.<sup>2</sup> All the aforementioned species display an outer blood–retina barrier (oBRB) formed by the retinal pigment epithelium (RPE),<sup>3</sup> which separates the neural retina from the fenestrated vascular system of the neighboring choroid. Whereas the endothelial iBRB has been shown to be essentially identical with the endothelial blood–brain barrier (BBB), comparative studies on barrier and carrier systems of the oBRB are fairly scarce.<sup>4</sup>

In contrast to the oBRB, the BBB is established by endothelial cells rather than by epithelial cells. In the brain, endothelial cells are induced, under the influence of astrocytes, to differentiate in a central nervous system (CNS)–specific manner,<sup>5</sup> whereas RPE cells in the eye are capable of producing barrier characteristics in the absence of astrocytes.<sup>3</sup> However, in both cases, expression of blood-barrier markers such as HT7/neurothelin and the endothelial barrier antigen EBA is strongly upregulated when barrier function is established during development.<sup>6–8</sup>

The intent of our comparative approach was a direct, detailed evaluation of the oBRB and BBB by pharmacologic and immunocytochemical means. We revealed unexpected similarities of drug permeation and transport systems in both blood barriers, which are of different ontogenetic origin. In addition, two major efflux systems were identified in the porcine oBRB for the first time.

## MATERIALS AND METHODS

Calcein AM (Molecular Probes, Eugene, OR), DAPI (4,6-diaminido-2-phenylindol, Sigma-Aldrich, Deisenhofen, Germany), dimethyl sulfoxide (DMSO; Sigma-Aldrich), Hanks' balanced salt solution (HBSS; PAA Laboratories, Cölbe, Germany), isopropanol, glutardialdehyde, paraformaldehyde (Merck, Darmstadt, Germany), BSA (bovine serum albumin), Triton X-100 (Sigma-Aldrich), sodium fluorescein (30 mM in H<sub>2</sub>O), memantine hydrochloride (1 mM in H<sub>2</sub>O), clonidine hydrochloride (6 mg/mL in H<sub>2</sub>O), cimetidine (6 mg/mL in H<sub>2</sub>O), rhodamine123 (0.4 mg/mL H<sub>2</sub>O), verapamil hydrochloride (1.5 mM in H<sub>2</sub>O), gabapentin (1.7 mM in H<sub>2</sub>O), probenecid (5  $\mu$ g/ $\mu$ L in DMSO), and atenolol (5  $\mu$ g/ $\mu$ L in ethanol) were used.<sup>9</sup> Gabapentin was provided by Schering AG (Berlin, Germany). Probenecid and atenolol were provided by Bayer AG (Leverkusen, Germany). Primary antibodies: rat anti ZO-1 (mAb 1520; Chemicon, Temecula, CA), mouse anti P-gp (mAb C-219), and polyclonal antibody to MRP

From the <sup>1</sup>NMI Natural and Medical Sciences Institute, University of Tübingen, Rütlingen, Germany; <sup>2</sup>Schering AG, Berlin, Germany; and <sup>3</sup>Bayer AG, Leverkusen, Germany.

Supported by the German Ministry of Education and Research (BMBF), Bayer AG, Abbott GmbH & Co. KG, Grünenthal GmbH, Merz Pharmaceuticals GmbH, and Schering AG.

Submitted for publication August 2, 2004; revised September 29 and October 27, 2004; accepted November 3, 2004.

Disclosure: **H. Steuer**, Bayer AG, Abbott GmbH & Co., Grünenthal GmbH, Merz Pharmaceuticals GmbH, Schering AG (F); **A. Jaworski**, Bayer AG, Abbott GmbH & Co., Grünenthal GmbH, Merz Pharmaceuticals GmbH, Schering AG (F); **B. Elger**, Schering AG (E, F) and Bayer AG, Abbott GmbH & Co., Grünenthal GmbH, Merz Pharmaceuticals GmbH, (F); **M. Kaussmann**, Bayer AG (E, F) and Abbott GmbH & Co., Grünenthal GmbH, Merz Pharmaceuticals GmbH, Schering AG (F); **J. Keldenich**, Bayer AG (E, F) and Abbott GmbH & Co., Grünenthal GmbH, Merz Pharmaceuticals GmbH, Schering AG (F); **H. Schneider**, Schering AG (E, F) and Bayer AG, Abbott GmbH & Co., Grünenthal GmbH, Merz Pharmaceuticals GmbH (F); **D. Stoll**, Bayer AG, Abbott GmbH & Co., Grünenthal GmbH, Merz Pharmaceuticals GmbH, Schering AG (F); **B. Schlosshauer**, Bayer AG, Abbott GmbH & Co., Grünenthal GmbH, Merz Pharmaceuticals GmbH, Schering AG (F)

The publication costs of this article were defrayed in part by page charge payment. This article must therefore be marked "advertisement" in accordance with 18 U.S.C. §1734 solely to indicate this fact.

Corresponding author: Burkhard Schlosshauer, NMI Natural and Medical Sciences Institute at the University Tübingen, Markwiesenstr. 55, D-72770 Rütlingen, Germany; schlosshauer@nmi.de.

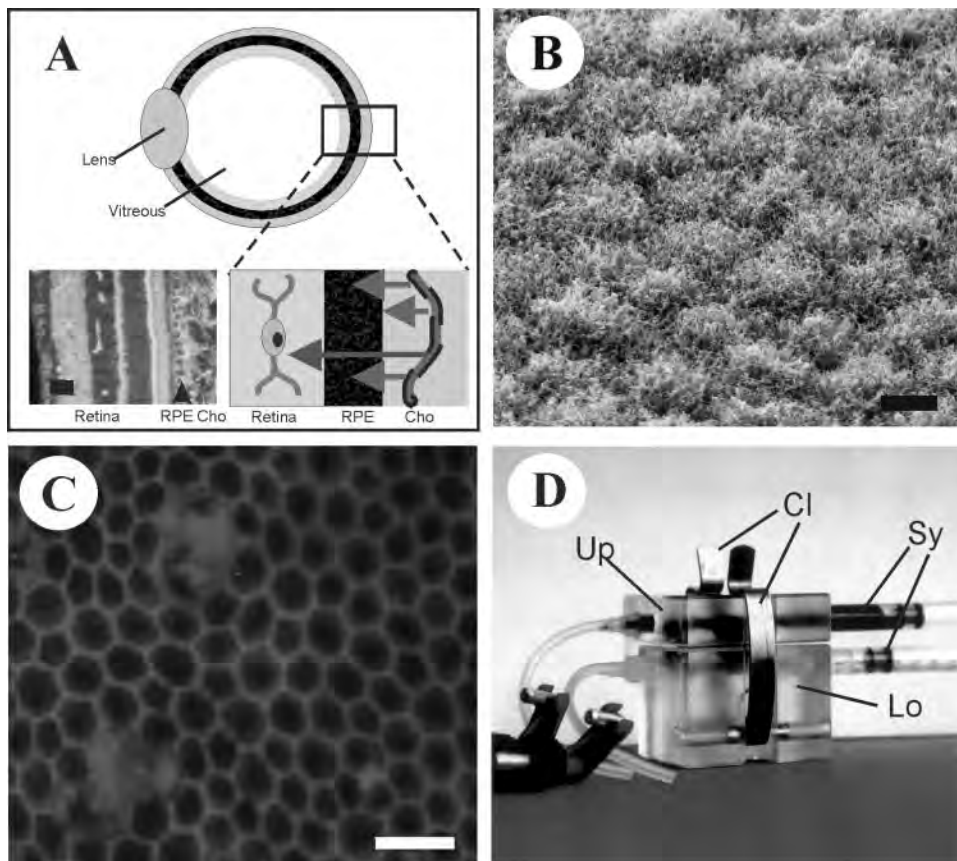


**FIGURE 1.** Retinal pigment epithelium and perfusion chamber. **(A)** Schematic representation of the eye, consisting of the lens, vitreous, retina, pigment epithelium, and choroid. The oBRB is formed by the pigment epithelium. *Left inset:* fluorescent phalloidin labeling of a retinal cross section with retina, RPE, and choroid (Cho) corresponding to the schematic (*right inset*). Diffusion/transport of blood-borne components (*arrows, right inset*) is controlled by the pigment epithelium. **(B)** Scanning electron micrograph of the retinal surface of the pigment epithelium. Epithelial microvilli remained intact during tissue preparation. **(C)** Immunofluorescence of the pigment epithelial wholmount showing the localization of the tight junction protein ZO-1. **(D)** Perfusion chamber with the donor compartment in the upper chamber (Up) and the donor compartment in the lower chamber (Lo). Both chambers are tightly sealed by compression with metal clamps (Cl). Application and collection of test solutions is performed with syringes (Sy) adapted to the corresponding in- and outlets of both chambers. Bars: **(B)** 10  $\mu\text{m}$ ; **(C)** 20  $\mu\text{m}$ .

(A23; both Alexis Biochemicals, San Diego, CA). Fluorescent mounting medium (Dako, Glostrup, Denmark). Secondary antibodies were: Cy2- and Cy3-conjugated goat anti-mouse and rat IgG and M and goat anti-rabbit IgG (Dianova/Jackson ImmunoResearch, Hamburg, Germany).

### oBRB Preparation

Enucleated porcine eyeballs were transported from the abattoir to the laboratory in ice-cold 0.9% NaCl. After muscle and connective tissues were removed from the bulbus, the anterior eye segment, sclera, and vitreous were removed, leaving the retina/RPE/choroid unaffected. The remaining tissue was flatmounted onto a paraffin-filled dissecting dish with fine needles. Retina/RPE sheets were freed from the underlying sclera with forceps and a microspatula. No comparative experiments were performed with the vitreous in place. (For simplicity, both RPE/choroid tissue sheets, with and without retina, are termed the *oBRB tissue sheet*.) The time necessary for transport and tissue dissection (all at 4°C) was typically in the range of 90 minutes. For viability and integrity studies, the retina was removed to allow for direct optical monitoring of the retinal pigment epithelium cell surfaces.

### oBRB Permeability Assay

oBRB tissue sheets were used as the interface between both compartments of a prewarmed perfusion chamber (Fig. 1). Closure of the chamber lid provided simultaneous immobilization of the oBRB tissue sheet and tight sealing of both compartments by virtue of two metal clamps. The diluted test agent/HBSS solutions were added to the donor chamber with a 1-mL syringe, whereas the acceptor chamber only contained HBSS. After 30 minutes at 37°C, solutions from the donor and acceptor chambers were collected and analyzed with HPLC/mass spectrometry (MS). The integrity of each tissue

sheet was tested. Only data from intact specimens were evaluated, as described recently.<sup>9</sup>

### Transfilter Coculture

Bovine brain capillary endothelial cells (BBCECs) were isolated from brains, purified, and cultured according to Mérésse et al.<sup>10</sup> Briefly, after mechanical homogenization, microvessels were seeded onto dishes coated with an extracellular matrix secreted by bovine corneal endothelial cells.<sup>11</sup> Colonies of endothelial cells were seeded onto gelatin-coated dishes. Astrocytes were prepared mechanically from cortices of newborn rats, as described by Booher and Sensenbrenner.<sup>12</sup> For cocultivation, confluent BBCECs of passage 4 to 6 were split from 60-mm dishes 1:100 onto rat tail collagen-coated filters (Transwell; Corning Costar, Corning, NY) and placed into 12-well plates containing astrocytes of passage 1 ( $4 \times 10^4$  cells/cm<sup>2</sup>).

For testing the BBB coculture's integrity, the permeability of [<sup>14</sup>C]-sucrose was determined every day before drug application. [<sup>14</sup>C]-sucrose at 1.0  $\mu\text{M}$  (specific activity between 486 and 643 mCi/mmol; Amersham, Freiburg, Germany) was added to the luminal (vascular) chamber and continuously mixed (universal shaker, ~140 rpm, 37°C; Bühler, Dresden, Germany). Fifty-microliter aliquots were collected at three time points both from the luminal and abluminal (brain) chamber. At  $t = 0$  and 30 minutes of the permeability study, aliquots were collected from the luminal chamber and quantified with a scintillation counter (Tri-Carb 1500; Canberra Packard, Dreieich, Germany). Endothelial monolayers were considered to represent a tight barrier, if the sucrose permeability was  $<1.0 \times 10^{-5}$  cm/sec. The amount of drugs passing through intact endothelial cell layers after 10, 20, and 30 minutes was quantified by HPLC analysis of samples taken from the abluminal side of the filter ( $n = 3$ ). Permeability calculations were performed according to the clearance principle.<sup>13,14</sup> Experiments were kindly performed at Merz Pharmaceuticals GmbH (Frankfurt, Germany).

## In Vivo Analysis and Determination of the Brain–Plasma Ratio

Drugs were formulated in saline containing 5% pluronic F68 and administered intraperitoneally to three separate groups ( $n = 3$ ) of male mice. Group A was killed after 0.5 hour, group B after 1 hour, and group C after 3 hours. The administration via the intraperitoneal route resulted in a slow absorption with peak plasma levels around 0.5 hour. The animals were killed by decapitation. This procedure ensures two options. First, there was no need for the use of anesthetics, which may impair the BBB and induce artifacts at higher brain levels. Second, blood flow was interrupted immediately, preventing any postmortem compound transition between systemic circulation and the brain. The time between interruption of blood flow by decapitation and freezing of the brain tissue at  $-20^{\circ}\text{C}$  ( $<2$  minutes) was unlikely to influence the drug concentration in the brain. The entire brain was taken for analysis, including  $\sim 2\%$  blood remaining in the vasculature. A correction for residual drugs in the blood was not applied, because it would have resulted only in a statistically insignificant change of the brain–plasma (BP) ratio of memantine, verapamil, and clonidine by 0.1% to 1.4%, which was beyond the standard deviation. For probenecid, the correction would have shifted the BP ratio from 0.05 to 0.03 (see the Results). Blood samples were collected in heparinized tubes. Brain homogenate (1:5 in 50 mM Tris-HCl [pH 7.5]) and plasma were precipitated (1:5) with acetonitrile containing an internal standard compound. After freezing and thawing, the supernatant was taken directly for liquid chromatography–tandem mass spectrometry (LC/MS/MS) quantification, using calibration curves in matrices. In vivo experimentation followed strictly the German and European Union guidelines regulating animal research and the ARVO Statement for the Use of Animals in Ophthalmic and Vision Research.

## HPLC Analysis

The HPLC system (at the Natural and Medical Sciences Institute [NMI]) was connected to a triple-quadrupole mass spectrometer (Quattro Micro; Micromass, Raleigh, NC) equipped with an electrospray ion source, or a fluorescence detector (model L 7400; Merck-Hitachi). To calculate the permeability coefficients of test compounds, the following formula was used:

$$P_e = dx/dt \times (C \times A)^{-1}$$

where  $P_e$  is the permeability coefficient (in centimeters per second),  $dx/dt$  is the rate of translocation (picomoles per second),  $C$  is the initial concentration of the drug in the donor chamber (in picomoles per cubic centimeter), and  $A$  is the area of penetration (in square centimeters).<sup>15</sup> Because the potential extracellular space (ECS) ( $<1\%$  of the tissue sheet) was considered to be negligible with five orders of magnitude less than the donor chamber volume, no correction concerning the ECS was made. Three independent experiments with six to eight specimens per application side and test agent were performed.

## Cytochemistry and Microscopy

oBRB tissue sheets were fixed in 4% paraformaldehyde at  $8^{\circ}\text{C}$  or in acetone at  $-20^{\circ}\text{C}$ . In some cases, oBRB tissue sheets were permeabilized with 0.1% Triton X-100 ( $22^{\circ}\text{C}$ , 30 minutes). After the application of primary antibodies, a carbocyanine-conjugated secondary antiserum (Cy2- or Cy3-conjugated goat anti-mouse/rat/rabbit IgG+M, 1:100 in 0.1% bovine serum albumin/PBS; Jackson ImmunoResearch/Dianova) was used (1 hour,  $22^{\circ}\text{C}$ ) to visualize antigen distribution. Specimens were also exposed to the DNA/nucleus stain DAPI (500 ng/mL PBS, 15 minutes,  $22^{\circ}\text{C}$ ). Control sections were incubated without antibodies or with only secondary antibodies.

For quantitative microscopy, oBRB tissue sheets were washed in HBSS and exposed to either verapamil (100  $\mu\text{M}$  in HBSS at  $37^{\circ}\text{C}$ , 30 minutes) or to control buffer (HBSS). All specimens were incubated concomitantly with calcein AM (1  $\mu\text{g}/\mu\text{L}$  DMSO diluted 1:200 in

HBSS). oBRB tissue sheets were washed twice with HBSS and inspected microscopically (Axiovert 35M, 10 $\times$  and 40 $\times$  Neofluar, 480 nm/ $>505$  nm; Carl Zeiss Meditec; Oberkochen, Germany). To determine potential endogenous fluorescence, specimens were monitored without addition of calcein. For the quantification of fluorescence of oBRB tissue sheets, image-analysis software was used (QWin; Leica Microsystems, Heidelberg, Germany).

For scanning electron microscopy, specimens were consecutively fixed in 4% paraformaldehyde (in PBS, 30 minutes,  $22^{\circ}\text{C}$ ) and 2% glutaraldehyde and 4% paraformaldehyde (in PBS, 16 hours,  $22^{\circ}\text{C}$ ).

## Statistics

If not stated otherwise, results are given as arithmetic means  $\pm$  SD of all samples of the same experimental specification. Because data did not fit to a normal distribution, the nonparametric Mann-Whitney test was used for significance calculations. Data were considered to be statistically significant when  $P < 0.01$ . For analysis, statistical software (StatView for Windows, ver. 5.0; SAS Institute, Cary, NC) was used.

## RESULTS

### The oBRB Model

As depicted in Figure 1A, blood-borne components originating from the sponge-like choroid pass through the retinal pigment epithelium (RPE) on their way to the neural retina. The porcine RPE is composed of a single layer of cells and appears as a continuous band of cells in cross sections of the eye (Fig. 1A, arrowhead in left inset; the multilayered retina is to the left, the unlayered choroid is to the right).

To control the state of the RPE after tissue processing, we removed the retina to allow direct visualization of the RPE surface. Scanning electron microscopy revealed that the RPE microvilli were indeed intact (Fig. 1B). Because we could not qualify cell–cell contacts in scanning electron micrographs, we also analyzed RPE wholemounts immunocytochemically with a specific antibody that binds to the tight junction protein ZO-1. Figure 1C shows a regular pattern of hexagonal cells. Of particular interest, neighboring cells were closely apposed, without loss of cell contacts. Controls without primary antibody but with secondary antibody did not display any unspecific staining (not shown). The data suggest that the overall tissue morphology remained unaffected by the dissection procedure, despite the fact that ZO-1 immunostaining alone cannot fully evaluate the integrity of the oBRB.

To analyze the physiological state of porcine oBRB preparations, we performed functional tests. RPE tissue sheets were immobilized in a two-chamber device (Fig. 1D) and were used as the interface between donor and acceptor chamber compartments. Both compartments could be hermetically sealed by closing the lid containing the donor chamber and latching it with metal clamps. Test solutions were added to and removed from the upper donor and lower acceptor chamber through syringes attached to the openings of both compartments (Fig. 1D). Sodium fluorescein was applied to the donor chamber as a tightness marker. Under our experimental conditions, only a minute amount of the marker compound permeated the oBRB, as reflected by the very low permeability coefficient ( $P_e$ ; see Fig. 3A). A  $P_e$  greater than  $5 \times 10^{-7}$  cm/sec was indicative of partially disrupted cell–cell contact sites in oBRB tissue sheets, as could be demonstrated by cytochemical means with calcein/propidium iodide double labeling.<sup>9</sup> oBRB specimens with a  $P_e$  greater than  $5 \times 10^{-7}$  cm/sec were excluded from further analysis. In summary, gentle and rapid organ processing provided morphologically and functionally intact oBRB tissue sheets.

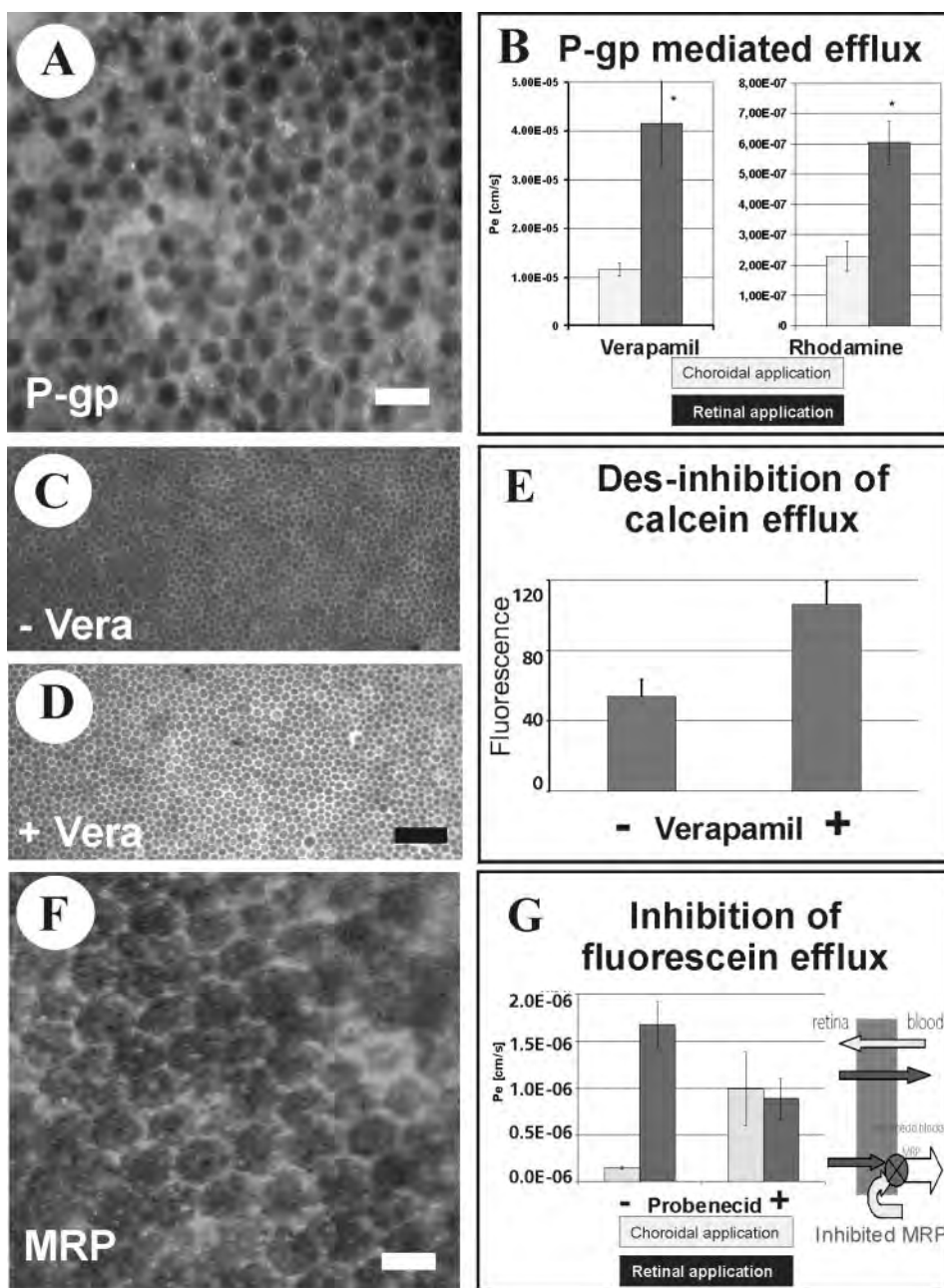


**FIGURE 2.** Efflux systems. (A) Immunofluorescence of the pigment epithelial wholemount showing the localization of P-gp. (B) Vectorial transport of the P-gp substrates verapamil and rhodamine 123. Application of these compounds to the retinal side of the oBRB resulted in a higher  $P_e$  than application to the choroidal side. This demonstrated a P-gp-mediated efflux from the neural tissue toward the blood ( $n = 22$  and  $30$ , respectively). (C, D) Calcein fluorescence of oBRB wholemounts in the presence or absence of competing verapamil ( $\pm$ Vera). (E) Quantification of fluorescence intensities revealed that competing verapamil resulted in higher calcein content in the cells, because calcein is also a P-gp substrate ( $n = 12$ ). Des-inhibition, abrogation of inhibition of calcein efflux. (F) Immunofluorescence of the pigment epithelial wholemount showing the localization of multidrug resistance-associated protein (MRP). (G) Vectorial transport of the MRP substrate fluorescein. Application of fluorescein to the retinal side of the oBRB produced a higher  $P_e$  than application of drugs to the choroidal side. This demonstrated an MRP-mediated efflux from the neural tissue toward the blood ( $n = 8$ ). Bars: (A)  $20 \mu\text{m}$ ; (D, applies to C)  $75 \mu\text{m}$ ; (F)  $10 \mu\text{m}$ .

### Efflux Systems

Two efflux systems were analyzed in a second set of experiments: the multidrug resistance protein P-gp and the multidrug-resistance-associated protein MRP. P-gp is a cell surface efflux pump found on the surfaces of endothelial cells in the BBB and helps to prevent entry of various biological components and pharmaceuticals into the brain parenchyma. For histologic analysis, oBRB tissue sheets were fixed and incubated with an anti-human P-gp rat antibody, which cross-reacts with porcine P-gp. As shown in Figure 2A, immunoreactivity was clearly evident and highlighted the positive cells in the hexagonal pattern typical of RPE cell morphology. Control staining with only the secondary antibody did not reveal any specific staining (data not shown).

The presence of a gene product does not necessarily imply that the immunocytochemically demonstrated antigen is biologically active. Consequently, we performed pharmacological

assays with two acknowledged P-gp substrates. oBRB tissue sheets were used as the barrier interface in the two-chamber device as described earlier, and verapamil and rhodamine 123 were applied either to the retinal or choroidal side of the oBRB. The determination of the resultant compound concentrations based on HPLC analysis revealed significant differences in apparent  $P_e$ , depending on the side of application (Fig. 2B). For both verapamil and rhodamine, higher permeabilities were observed in the retina-to-choroid (ret $\rightarrow$ cho) direction than in the opposite direction. The difference in apparent permeabilities between both directions was 3.5-fold for verapamil and 2.6-fold for rhodamine 123. Because for both test agents a higher apparent  $P_e$  was evident in the ret $\rightarrow$ cho direction, it can be concluded that P-gp is expressed in the oBRB and that P-gp is preferentially located on the choroidal side of the oBRB.

The efflux system was further investigated by using calcein as a third P-gp substrate in competition experiments. Normally,

calcein is internalized and becomes entrapped in viable cells after enzymatic cleavage, a process that can be quantified by the resultant intracellular fluorescence. However, if cells express P-gp, fluorescence remains at low levels due to the export of calcein from the cells by P-gp. To take advantage of this mechanism, oBRB tissue sheets were exposed to fluorescent calcein, either in the presence or absence of competitive nonfluorescent verapamil. In the absence of verapamil, only low levels of cell fluorescence were evident (Fig. 2C), whereas the presence of verapamil increased cell fluorescence (Fig. 2D). It is unknown whether intracellular calcein accumulation was accompanied by cell swelling. Fluorescence quantification by image analysis confirmed the qualitative impression: in the presence of verapamil the calcein labeling was twice as strong (mean gray values:  $106.3 \pm 13.0$  [SD] vs.  $53.8 \pm 9.7$  (SD);  $P < 0.01$ ). The data corroborated the finding that P-gp represents a functional efflux system in the oBRB.

The second type of efflux pump investigated belongs to the class of MRPs genetically different from P-gp. Immunocytochemistry of oBRB specimens with corresponding polyclonal antibodies showed that the oBRB also expressed MRP (Fig. 2F). Control staining with the secondary antibody alone did not reveal any specific staining (data not shown). To analyze further whether MRP was biologically active, we used native oBRB tissue sheets in the two-chamber device. The known MRP substrate fluorescein was applied to both sides of the oBRB in separate experiments. HPLC analysis revealed a 11.3-fold difference in apparent permeabilities ( $P < 0.01$ ) with a higher  $P_e$  in the ret→cho direction than in the cho→ret direction (Fig. 2G). In final experiments, MRP was pharmacologically blocked by coapplication of probenecid, with the result that  $P_e$  was equalized in both directions ( $P = 0.87$ ). The data are interpreted in mechanistic terms as an overlap of at least two basic types of oBRB permeation: one potentially based on MRP-independent diffusion (Fig. 2G, right insert, top bidirectional arrows) and one representing active, directed transport via MRP. The latter case increased the ret→cho flux, while decreasing ret→cho passage. In the presence of competing probenecid, MRP-mediated fluorescein transport was inhibited (Fig. 2G right inset, lower unidirectional arrows; crossed circle represents the inhibited MRP). As is true of all transport phenomena, other transport mechanisms cannot be excluded to date (see the Discussion section). However, the experimental observations are in agreement with the interpretation that the oBRB expresses MRP and MRP is likely to be located on the choroidal side of the oBRB.

### oBRB-BBB Comparison

For comparison of the oBRB model with a BBB in vitro model, nine different test compounds were used in parallel. Application of test agents in the two-chambered device and subsequent LC/MS/MS were performed as described herein. As an in vitro BBB model, a modified transfilter coculture system with bovine brain endothelial cells and astrocytes (BBCEC-ACs) was used. Astrocytes and brain endothelial cells were separately purified, cryopreserved, and cocultivated. Because of regulatory cell interactions, endothelial cells are induced to express BBB characteristics. As with the two-compartment device used for acute oBRB tissue sheets, samples can be applied separately to and collected from both sides of the barrier culture.

Because direct comparison of barrier permeation data (i.e., absolute numbers) is not possible, we compared the ranking (i.e., the relative permeabilities) of the compounds. The test compounds comprised memantine, verapamil, clonidine, gabapentin, probenecid, cimetidine, rhodamine 123, sodium fluorescein, and atenolol. These compounds represented different permeability classes, as has been outlined using 10 different

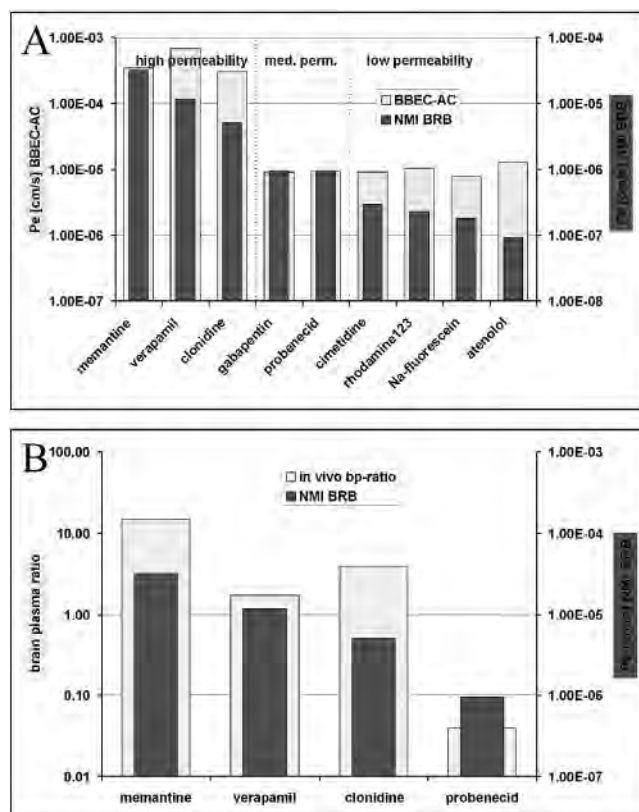


**FIGURE 3.** In vitro–in vivo oBRB/BBB comparison. (A) Comparison of oBRB tissue sheets used as the interface in the perfusion system (NMI BRB, dark shading) and a transfilter coculture system with purified bovine brain endothelial cells and astrocytes (BBCEC-AC, light shading).  $P_e$  was determined by MS and fluorescence detection. (B) Comparison of the  $P_e$  of different compounds determined with oBRB tissue sheets used in a perfusion chamber and of the BP ratio in mice. All three systems displayed somewhat similar ranking of test agent permeabilities.

test agents.<sup>9</sup> The first objective was to identify the dynamic range of detection addressable by the oBRB model. Considering the highest and lowest  $P_e$  measured ( $3.2 \times 10^{-5}$  and  $9.1 \times 10^{-8}$  cm/sec), the dynamic range covered more than two orders of magnitude (Fig. 3A). Within this range, three major categories can be classified by virtue of the oBRB model: poor permeation of approximately  $10^{-7}$  cm/sec, moderate permeation of approximately  $10^{-6}$  cm/sec, and pronounced permeation of approximately  $10^{-5}$  cm/sec. Comparison with the BBB in vitro model revealed a similar ranking of test compounds in both systems. The oBRB model allowed differentiation between compounds with medium permeation (e.g., the CNS drug gabapentin) and compounds with low permeation such as sodium fluorescein. The increased apparent  $P_e$  for verapamil in the BBCEC-AC model may be due to reduced expression of P-gp after long-term culturing. The dynamic range in the BBCEC-AC model covered  $P_e$  from  $8.00 \times 10^{-6}$  to  $6.75 \times 10^{-4}$  cm/sec.

The ultimate comparison included an in vivo paradigm based on the extra vascular (intraperitoneal) application of test compounds and the subsequent collection of blood and brain tissue. After mass spectrometry, BP ratios were calculated to provide an index of BBB permeation. For each compound, the BP ratios did not differ significantly between the three time points measured. The system covered a dynamic range of more than two orders of magnitude (0.04–15.00). Ranking of observed BP ratios for four test compounds revealed equivalent

data sets for the oBRB model and in vivo model (Fig. 3B). Though the ranking order of verapamil and clonidine was nominally inverted in the two models, this was not significant in view of the variance in the  $P_e$  and the small group size of the in vivo data. Most important, however, both agents were classified as high-permeability components in vivo and in the oBRB model. The ranking of test agents was identical at all three time points. Figure 3B depicts the 0.5 hour data, which is the same time point chosen for the oBRB system. In conclusion, the oBRB displayed pharmacological barrier and carrier characteristics comparable to the BBB, as demonstrated by the application of defined drugs in three model systems.

## DISCUSSION

### P-gp Efflux System

The fact that P-gp has become an important factor in drug development and medical care led us to address preferentially the efflux systems such as P-gp in our studies. P-gp hinders many medical treatments by conferring MDR on tumor and endothelial cells by transporting therapeutics out of these cells.<sup>16</sup> Chemosensitizers are thought to bind to the same active site as regular substrates, but their much higher rate of spontaneous flip-flop across the membrane may result in futile cycling of the transporter, preventing removal of coapplied P-gp substrates by the efflux mechanism. With regard to the medical implications, it was of pivotal interest to determine whether the oBRB displayed MDR activity.

Our data provided three types of evidence that P-gp is expressed in the oBRB. First, immunocytochemistry identified antigen expression in oBRB tissue sheets. Second, in pharmacological assays P-gp substrates displayed a vectorial flux toward the choroid. Third, quantitative fluoromicroscopy revealed that efflux of calcein was reduced by the P-gp chemosensitizer verapamil.

The data obtained in the oBRB system are very similar to BBB data. In the BBB, P-gp was localized on the luminal side of capillary endothelial cells in both the gray and white matter of the brain.<sup>17</sup> Brain microdialysis revealed that in *mdr1a*<sup>-/-</sup> mice lacking P-gp, the rhodamine 123 concentration in the brain parenchyma was four times higher than in wild-type mice.<sup>18</sup> This factor is in the same range as the vectorial difference we observed for rhodamine 123 in the porcine oBRB.

Published reports of oBRB P-gp expression oBRB remain scarce and controversial. P-gp immunoreactivity has been reported for the rat pigment epithelium,<sup>19</sup> whereas human specimens were claimed to be essentially P-gp negative.<sup>20</sup> However, P-gp expression was evident in 10 cases investigated after exposure to daunomycin, which had been prescribed for the management of proliferative vitreoretinopathy.<sup>20</sup> This raises the question of whether the initial failure to detect P-gp in most untreated specimens was due to a detection problem. Only a minor increase in *mdr-1* mRNA was detected after daunomycin treatment, implying primarily translational rather than transcriptional regulation of P-gp expression. In contrast to the data from Tervooren et al.,<sup>20</sup> another report demonstrated P-gp mRNA in untreated human native oBRB tissue and cultured RPE cells derived thereof.<sup>21</sup>

### MRP Efflux System

The second efflux system addressed in our study is the MRP.<sup>22</sup> Pathophysiologically, MRPs are of particular interest because, for example, of their overexpression in patients with pharmacoresistant epilepsy.<sup>23</sup> Because MRPs are likely to export anti-epileptic drugs such as carbamazepine from the brain, coapplication of MRP inhibitors is a promising means to overcome resistance.<sup>24</sup> Probenecid is an inhibitor of organic ion transport

and particularly blocks activity of MRP. Application of fluorescein in the presence of probenecid in the porcine oBRB model clearly demonstrated that the vectorial flux of fluorescein could be abrogated. This is in accordance with studies of the ARPE-19 cell line originating from the human retinal pigment epithelium, where the presence of the MRP inhibitor probenecid increased fluorescein accumulation.<sup>25</sup> Parallel to MRP efflux, organic anion transporter (Oat1 and Oat3) may also be active in the RPE. Both transporters have been shown to be located in the BBB, where they transport fluorescein and are inhibited by probenecid.<sup>26,27</sup> In addition to the pharmacological evidence, we demonstrated MRP antigen expression by immunocytochemical means. To our knowledge, this is the first evidence of MRP localization in the porcine oBRB that parallels expression in the endothelial BBB.

### oBRB–BBB Comparison

For the comparison of the oBRB model with established BBB models, we selected test compounds according to published transport specificity, structural-, ClogP-, and BBB-permeation data. The BBB crossing characteristics ranged from high (e.g., memantine; ClogP 2.8) to very low (e.g., atenolol, ClogP -1.1) permeation. Several of the selected compounds (e.g., cimetidine, probenecid, fluorescein, rhodamine, and gabapentin) are known to be subject to different transport mechanisms at the BBB, whereas others (e.g., memantine, a glutamate receptor blocker, and atenolol, a  $\beta$ -blocker for the treatment of hypertension) exhibit only physical permeation across the BBB.

To avoid artifacts typically observed in single-cell cultures, such as cellular dedifferentiation or loss of cell polarity and tight junctions, the most advanced transfilter coculture system presently available was used as a BBB in vitro model.<sup>28</sup> This system is composed of BBECs placed on semipermeable membranes and spatially separated rat astrocytes.<sup>14</sup> The permeation ranking of test compounds was similar in the oBRB and BBB in vitro system, though the cell-based in vitro model did not display the same dynamic range and resolution as the intact acute tissue preparation or the in vivo model. Also in the in vivo model, all test compounds were classified in the same permeability categories as in the oBRB system.

Although cell death and subsequent leakage of the BBB may have occurred in vivo within 2 minutes of animal death, as has been found in another study with a novel noninvasive approach, using the contrast agent gadolinium derivative Gd-DTPA together with dynamic contrast enhanced magnetic resonance imaging (DCE-MRI),<sup>29</sup> it is unlikely that the test agent classification would have been different from that calculated in the current study. Nevertheless, it cannot be ruled out that in both oBRB and BBB in vitro systems the induction of cell death was different from that in vivo.

## CONCLUSION

In summary, our data, based on a broad range of test agents, provide evidence that the epithelial oBRB mirrors the pharmacologic properties of the endothelial BBB to a large extent and expresses the same major efflux systems. This aspect is of interest also because a magnitude of cellular, structural, and functional differences between the oBRB and BBB are evident. From an ontogenetic point of view, it cannot be assumed that both blood barriers serve to control homeostasis of neuronal parenchyma in a similar way. The endothelial BBB is of mesenchymal origin, whereas the retinal pigment epithelium derives from the neuroectoderm.<sup>30,31</sup> The BBB is formed after immigration of angioblasts into the neural parenchyma,<sup>32</sup> in contrast to pigment epithelial cells, which from the earliest stages of neuroembryonic development represent a monocel-

lular layer neighboring the transient optic ventricle.<sup>33</sup> The completely different origins result in morphologically clearly discernible cell types and organ structures. Consequently, it comes as a surprise that equivalent functional entities with regard to the discussed barrier/carrier characteristics are evident in both locations. For the first time it was shown that the porcine oBRB expresses the two major efflux systems—P-gp (MDR) and MRP—in a polarized fashion that results in directed drug transport.

### Acknowledgments

The authors thank Anette Bartmann (formerly with Merz Pharmaceuticals GmbH), Tanja Bauer (Merz Pharmaceuticals GmbH), Horst Beyer (Grünenthal GmbH), Raymond Butts (NMI), Thomas Carl (University of Tuebingen), Joerg Delzer (Abbott GmbH & Co. KG), Nadja Gugeler (NMI), Guenther Quack (Merz Pharmaceuticals GmbH), Willi Schmitt (Bayer AG), and Meik Sladek (Merz Pharmaceuticals GmbH) for stimulating discussions, experimental support, quantitative analysis of test agents, and correcting the manuscript; and Elvira Bublitz, Silvia Engert, Norbert Kern, and Iris Seybold (all NMI) for excellent technical assistance.

### References

- Bradbury MWB. The blood-brain barrier. *Exp Physiol.* 1993;78:453–472.
- Kupersmith MJ, Shakib M. The blood-ocular barrier. In: Neuwelt EA, ed. *Implications of the Blood-Brain Barrier and Its Manipulation*. New York: Plenum; 1989;369–390.
- Marmor MF. Comparative and evolutionary aspects of the retinal pigment epithelium. In: Wolfensberger TJ, ed. *The Retinal Pigment Epithelium*. Oxford, UK: Oxford University Press 1998;23–37.
- Schlosshauer B, Steuer H. Comparative anatomy, physiology and in vitro models of the blood-brain- and blood-retina barrier. *Curr Med Chem.* 2002;2:175–186.
- Janzer RC, Raff MC. Astrocytes induce blood-brain barrier properties in endothelial cells. *Nature.* 1987;325:253–257.
- Lawrenson JG, Ghabriel MN, Reid AR, Gajree TN, Allt G. Differential expression of an endothelial barrier antigen between the CNS and the PNS. *J Anat.* 1995;186:217–221.
- Schlosshauer B, Herzog K-H. Neurothelin: an inducible cell surface glycoprotein of blood-brain barrier-specific endothelial cells and distinct neurons. *J Cell Biol.* 1990;110:1261–1274.
- Ikeda E, Flamme I, Risau W. Developing brain cells produce factors capable of inducing the HT7 antigen, a blood-brain barrier-specific molecule, in chick endothelial cells. *Neurosci Lett.* 1996;209:149–152.
- Steuer H, Jaworski A, Stoll D, Schlosshauer B. In vitro model of the outer blood-retina barrier. *Brain Res Protoc.* 2004;13:26–36.
- Meresse S, Dehouck M-P, Delorme P et al. Bovine brain endothelial cells express tight junctions and monoamine oxidase activity in long-term cultures. *J Neurochem.* 1989;53:1363–1371.
- Gospodarowicz D, Moran J, Braun D, Birdwell C. Clonal growth of bovine vascular endothelial cells: fibroblast growth factor as a survival agent. *Proc Natl Acad Sci USA.* 1976;73:4120–4124.
- Booher J, Sensenbrenner M. Growth and cultivation of dissociated neurons and glial cells from embryonic chick, rat and human brain in flask cultures. *Neurobiology.* 1972;2:97–105.
- Siflinger-Birnboim A, Del Vecchio PJ, Cooper JA, Blumenstock FA, Shepard JM, Malik AB. Molecular sieving characteristics of the cultured endothelial monolayer. *J Cell Physiol.* 1987;132:111–117.
- Dehouck B, Cecchelli R, Dehouck M-P. A co-culture of brain capillary endothelial cells and astrocytes: an in vitro blood-brain barrier for studying drug transport to the brain. In: Sutanto W, ed. *Drug Transport across the Blood-Brain Barrier*. Amsterdam, The Netherlands: Harwood Academic; 1998.
- Letrent SP, Polli JW, Humphreys JE, Pollack GM, Brouwer KR, Brouwer KLR. P-glycoprotein-mediated transport of morphine in brain capillary endothelial cells. *Biochem Pharmacol.* 1999;58:951–957.
- Sharom FJ. The p-glycoprotein efflux pump: how does it transport drugs? *J Membr Biol.* 1997;160:161–175.
- Kang YS, Terasaki T, Ohnishi T, Tsuji A. In vivo and in vitro evidence for a common carrier mediated transport of choline and basic drugs through the blood-brain barrier. *J Pharmacobiol Dyn.* 1990;13:353–360.
- de Lange ECM, de Bock G, Schinkel AH, de Boer AG, Breimer DD. BBB transport and p-glycoprotein functionality using MDR1A(–/–) and wild type mice: total brain versus microdialysis concentration profiles of rhodamine-123. *Pharm Res.* 1998;15:1657–1665.
- Holash JA, Stewart PA. The relationship of astrocyte-like cells to the vessels that contribute to the blood-ocular barriers. *Brain Res.* 1993;629:218–224.
- Tervooren D, Heimann K, Bartz-Schmidt KU, Walter P, Weller M. Intravitreal daunomycin induces multidrug resistance in proliferative vitreoretinopathy. *Invest Ophthalmol Vis Sci.* 1998;39:164–170.
- Kennedy BG, Mangini NJ. P-glycoprotein expression in human retinal pigment epithelium. *Mol Vis.* 2002;8:422–430.
- Kruh GD, Zeng H, Rea PA, et al. MRP subfamily transporters and resistance to anticancer agents. *J Bioenerg Biomembr.* 2001;33:493–501.
- Abbott NJ, Khan EU, Rollinson CMS. Drug resistance in epilepsy; role of the blood brain barrier. In: Ling V, ed. *Mechanisms of Drug Resistance in Epilepsy. Lessons from Oncology*. Chichester, UK: Wiley; 2001.
- Potschka H, Fedrowitz M, Löscher W. P-glycoprotein and multidrug resistance-associated protein are involved in the regulation of extracellular levels of the major antiepileptic drug carbamazepine in the brain. *Neuroreport.* 2001;12:3557–3560.
- Aukunuru JV, Sunkara G, Bandi N, Thoreson WB, Kompella UB. Expression of multidrug resistance-associated protein (MRP) in human retinal pigment epithelial cells and its interaction with BAPSG, a novel aldose reductase inhibitor. *Pharm Res.* 2001;18:565–572.
- Dantzer WH, Wright SH. The molecular and cellular physiology of basolateral organic anion transport in mammalian renal tubules. *Biochim Biophys Acta.* 2003;1618:185–193.
- Sugiyama D, Kusuhara H, Shitara Y, et al. Characterization of the efflux transport of 17beta-estradiol-D-17beta-glucuronide from the brain across the blood-brain barrier. *J Pharmacol Exp Ther.* 2001;298:316–322.
- Terasaki T, Ohtsuki S, Hori S, Takanaga H, Nakashima E, Hosoya K. New approaches to in vitro models of blood-brain barrier drug transport. *Drug Discov Today.* 2003;8:944–954.
- Berkowitz BA, Roberts R, Luan H, Peysakhov J, Mao X, Thomas KA. Dynamic contrast-enhanced MRI measurements of passive permeability through blood retinal barrier in diabetic rats. *Invest Ophthalmol Vis Sci.* 2004;45:2391–2398.
- Mund ML, Rodrigues MM. Embryology of the human retinal pigment epithelium. In: Marmor MF, ed. *The Retinal Pigment Epithelium*. Cambridge, MA: Harvard University Press; 1979;45–52.
- Coulombre AJ. Roles of the retinal pigment epithelium in the development of ocular tissues. In: Marmor MF, ed. *The Retinal Pigment Epithelium*. Cambridge, MA: Harvard University Press; 1979;53–57.
- Risau W. Mechanisms of angiogenesis. *Nature.* 1997;386:671–674.
- Rizzolo LJ. Polarity and the development of the outer blood-retinal barrier. *Histol Histopathol.* 1997;12:1057–1067.